JOURNAL OF MATERIALS SCIENCE 23 (1988) 1036–1041

Electrical properties and microstructure in the system ceria–alkaline earth oxide

HIDENORI YAHIRO, TATSUYA OHUCHI, KOICHI EGUCHI, HIROMICHI ARAI*
Department of Materials Science and Technology, Graduate School of Engineering Sciences, Kyushu University 39, Kasugakoen, Kasuga-shi, Fukuoka 816, Japan

The ionic conduction of oxygen in the ceria–alkaline earth oxide system was investigated as a function of temperature, partial pressure of oxygen and oxide composition, together with its crystal structure, density, and microstructure. Undoped ceria and its solid solution with alkaline earth oxides have a cubic fluorite structure. The ionic conductivity of ceria is greatly enhanced by additions of calcia and strontia, even when they are added in excess of the solubility limit. The conductivities of ceria–calcia and ceria–strontia were much higher than those of calcia- and yttria-stabilized zirconia. Up to the limit of calcia and strontia, the ionic transference number was nearly unity in the temperature range between 600 and 900° C. With an increase in calcia and strontia content, the ionic conductivity was little affected by the presence of a second phase of CaO and $SrCeO_3$.

1. Introduction

Solid electrolytes with a high ionic conduction of oxygen have been attracting great interest for application in high-temperature fuel cells [1, 2] and oxygen sensors [3]. The materials used for these purposes are fluorite-type oxides which are doped with divalent or trivalent cations so as to introduce a high concentration of oxygen vacancies [4, 5]. Stabilized zirconia has been investigated as a popular solid electrolyte [6]; however, its conductivity is insufficient to derive the desired output for a fuel cell. There is much interest in the use of cation-doped ceria, which possesses a much higher ionic conductivity than stabilized zirconia, as several investigators have reported previously [7]. A series of cations in oxide form, such as CaO [8, 9], SrO [10, 11], Y_2O_3 [4, 12] and rare-earth oxides [13–15] were investigated as dopants for CeO_2. It is reported that a part of the alkaline earth oxides were soluble in the ceria lattice resulting in the formation of oxygen vacancies; however, the electrochemical properties of alkaline earth oxide-doped ceria have not been fully reported as a function of additive content. In the present paper, the electrical conductivity and ionic transference number of the ceria–alkaline earth oxide systems are investigated and discussed in terms of the crystal structure, density, and microstructure.

2. Experimental procedure

2.1. Sample preparation

Polycrystalline powder was prepared from cerium dioxide and alkaline earth oxide or carbonate. The calculated amount of CeO_2 (99.9%) and $CaCO_3$ (99.0%), $SrCO_3$ (99.9%), $BaCO_3$ (99.9%) or MgO (99.99%) mixture was milled overnight with urethane balls and calcined at 1300° C for 10 h. The oxide powders were pressed into a compact (20 mm in diameter and 2 to 5 mm in thickness) axially at 1 to 2.5 × 10^3 kg cm^{-2} and isostatically at 2.7 × 10^3 kg cm^{-2}. The disc was finally sintered at 1450 or 1650° C for 15 h in air.

The density of the sintered disc was determined by a water pycnometric technique. The crystal structure was determined at room temperature by X-ray diffraction using Cu$K\alpha$ radiation after crushing the discs into powders. Sodium chloride crystals were used as an internal standard for diffraction angles.

2.2. Measurement of ionic transference number of oxygen

The mean ionic transference number, t_i, is given by

$$t_i = E_{obs} \Big/ \left[\frac{RT}{4F} \ln\left(\frac{P''_{O_2}}{P'_{O_2}}\right)\right] \quad (1)$$

where E_{obs} stands for the observed e.m.f. of the following cell:

$$P'_{O_2}, \text{ Pt/solid electrolyte/Pt, } P''_{O_2} \quad (2)$$

In the present measurements, P'_{O_2} was fixed at 1 atm and the e.m.f. was obtained as a function of P''_{O_2} (1.0×10^{-3} to 0.21 atm). The electromotive force of a gas concentration cell was measured in a temperature range between 600 and 900° C with a gas flow rate of 200 to 300 cm^3 min^{-1}. On each flat surface of a cylindrical disc, a platinum paste (Tanaka Matthey KT-5, Tokyo) was applied as an electrode and fired at 1000° C for 10 min to obtain an electrical contact. The disc was attached to a mullite tube by fusion welding of silver to ensure the gas-tightness of the cell at elevated temperatures.

*To whom correspondence should be addressed.

0022–2461/88 $03.00 + .12

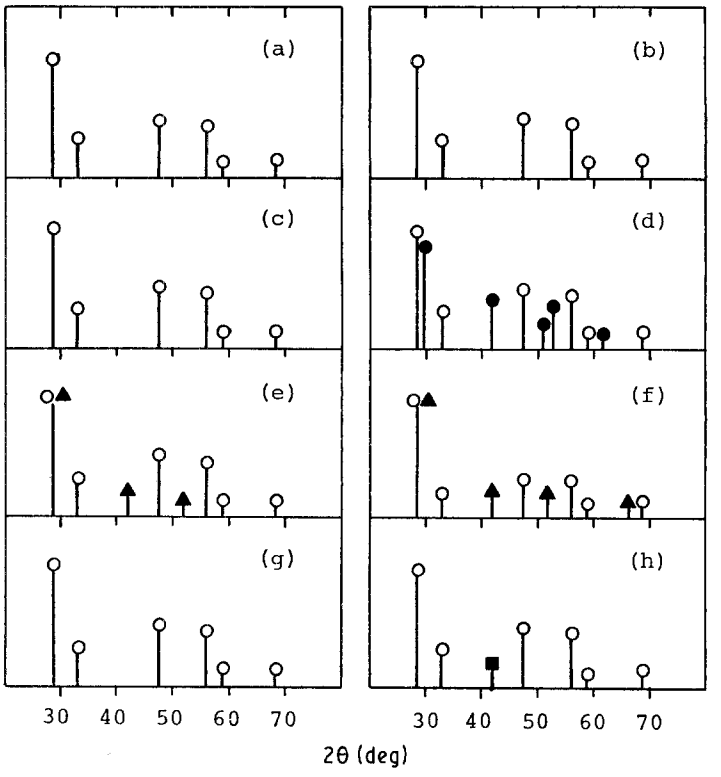

Figure 1 X-ray diffraction patterns of $(CeO_2)_{1-x}(MO)_x$: (a) $(CeO_2)_{0.90}(CaO)_{0.10}$, (b) $(CeO_2)_{0.70}(CaO)_{0.30}$, (c) $(CeO_2)_{0.90}(SrO)_{0.10}$, (d) $(CeO_2)_{0.70}(SrO)_{0.30}$, (e) $(CeO_2)_{0.90}(BaO)_{0.10}$, (f) $(CeO_2)_{0.70}(BaO)_{0.30}$, (g) $(CeO_2)_{0.90}(MgO)_{0.10}$, (h) $(CeO_2)_{0.70}(MgO)_{0.30}$. (○) Fluorite-type structure of CeO_2, (●) perovskite-type structure of $SrCeO_3$, (▲) perovskite-type structure of $BaCeO_3$, (■) rocksalt-type structure of MgO.

2.3. Measurement of electrical conductivity

The electrical conductivity of a sintered sample (15 mm × 4 mm × 5 mm) was measured by a conventional d.c. four-probe method. Electric contacts between current probes and the sample were made by platinum wires and paste. A galvanostatic d.c. source was used to supply current to these probes. Potential probes were located between two current probes by tightly winding platinum wires around the sample. The potential drop between two potential probes was measured with a digital voltmeter. Ionic conductivity was assumed to be the product of the observed conductivity and the ionic transference number.

2.4. Microstructure of samples

Microstructures at the fracture surfaces of ceria-based oxides were observed by SEM (Jeol JSM-10A). The compositions of CeO_2–SrO systems were observed with a Jeol JXA-5A electron microanalyser. The samples were polished with a diamond suspension prior to the measurement. The back-scattered electron image and X-ray image were obtained to determine the distribution of phases and components.

3. Results and discussion

3.1. Crystal structure and phases of sintered samples

Dissolution of alkaline earth metal in a ceria crystal leads to the quantitative formation of oxygen vacancies because of charge compensation. Phases in the sintered specimens and the solubility of the additive were measured by X-ray diffraction. Pure CeO_2 and alkaline earth oxides have the fluorite and rocksalt structures, respectively. Fig. 1 shows X-ray diffraction patterns of ceria–alkaline earth oxide systems. Hereafter, the sample composition is expressed as a molar fraction of alkaline earth oxide, x, i.e. $(CeO_2)_{1-x}(MO)_x$ (M = Ca, Sr, Ba, Mg). The diffraction pattern of pure CeO_2 consisted of lines from the cubic fluorite structure. The lattice constant (a = 0.541 nm) agreed well with the reported value. The diffraction patterns of $(CeO_2)_{0.90}(CaO)_{0.10}$, $(CeO_2)_{0.90}(SrO)_{0.10}$ and $(CeO_2)_{0.90}(MgO)_{0.10}$ are essentially unchanged from that of pure CeO_2 except for slight shifts in diffraction angles. These shifts are due to dissolution of the additives in the fluorite lattice. The diffraction angles of $(CeO_2)_{0.90}(BaO)_{0.10}$ also shifted and diffraction peaks of $BaCeO_3$ with a perovskite structure were superposed on those of the fluorite structure.

A precipitated second phase was contained in every sample at x = 0.30 in addition to the fluorite phase. Perovskite-type oxides of $SrCeO_3$ and $BaCeO_3$ were precipitated for $(CeO_2)_{0.70}(SrO)_{0.30}$ and $(CeO_2)_{0.70}(BaO)_{0.30}$, whereas rocksalt-type oxides of CaO and MgO were precipitated for $(CeO_2)_{0.70}(CaO)_{0.30}$ and $(CeO_2)_{0.70}(MgO)_{0.30}$.

The lattice constant of the fluorite structure is plotted as a function of oxide composition in Fig. 2. With increasing CaO content, the lattice constant increased linearly up to x = 0.23, but the value was almost constant at $x > 0.3$. The plots indicate that the solubility limit of CaO in CeO_2 is about 23 mol %, in agreement with that reported by Longo and Podda [16].

The lattice constant increased very steeply with increasing SrO content, but the solubility limit was about 8 mol %. Although the lattice constant of MgO- and BaO-doped ceria also deviated from that of undoped ceria, their solubility limits were too small to be determined. The solubilities of alkaline earth oxides as well as the change in lattices parameters can be qualitatively explained by the sizes of the cations. The ionic radii of Ce^{4+}, Mg^{2+}, Ca^{2+}, Sr^{2+} and Ba^{2+} are reported as 0.097, 0.089, 0.112, 0.125, and 0.142 nm, respectively. Additives with ionic radii close to that of the cerium cation, especially Ca^{2+}, are very soluble.

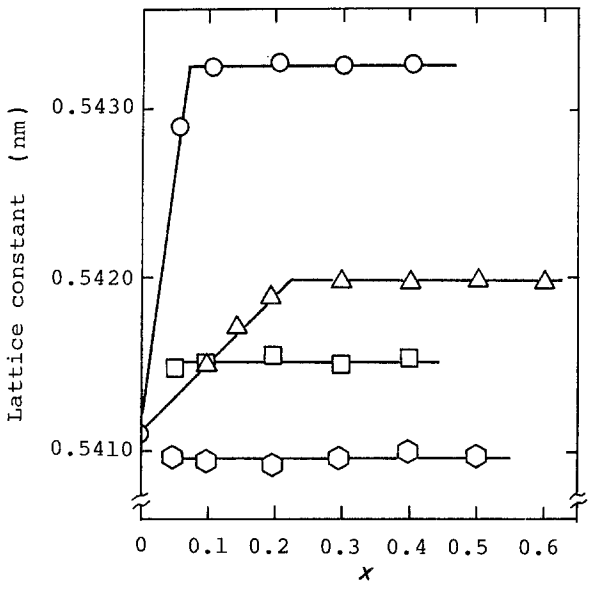

Figure 2 Lattice constant of ceria–alkaline earth oxide systems as a function of content of dopant: (○) $(CeO_2)_{1-x}(SrO)_x$, (△) $(CeO_2)_{1-x}(CaO)_x$, (□) $(CeO_2)_{1-x}(BaO)_x$, (○) $(CeO_2)_{1-x}(MgO)_x$.

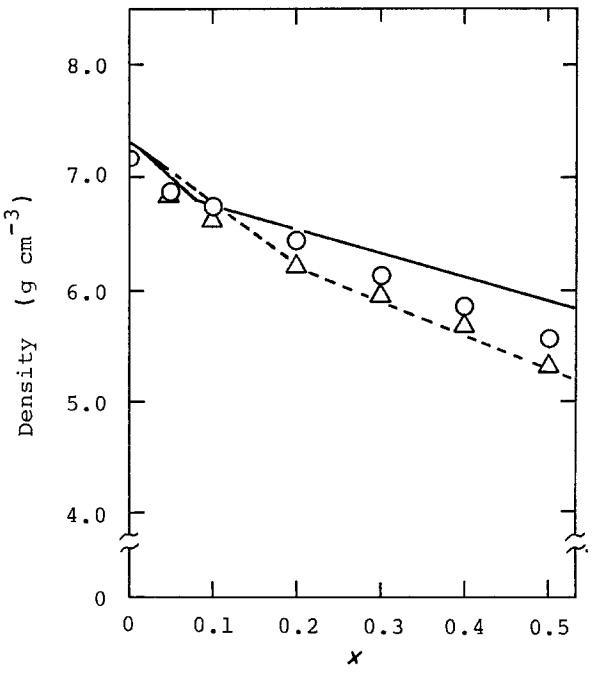

Figure 3 Densities of sintered CeO_2–SrO and CeO_2–CaO systems: (○) $(CeO_2)_{1-x}(SrO)_x$, (△) $(CeO_2)_{1-x}(CaO)_x$, (——) calculated density of $(CeO_2)_{1-x}(SrO)_x$, (– – –) calculated density of $(CeO_2)_{1-x}(CaO)_x$.

The crystal lattice expands or shrinks depending on whether the ionic radius is larger or smaller, respectively, than that of cerium. A large solubility results in a great number of oxygen vacancies in the fluorite lattice. In a separate experiment, some rare earth oxides such as Yb_2O_3, Gd_2O_3 and Sm_2O_3 with ionic radii close to that of Ce^{4+} were much more soluble in ceria than alkaline earth oxides.

Fig. 3 shows the density of sintered CeO_2–SrO and CeO_2–CaO. The broken line and dotted line in this figure represent theoretical densities which are calculated from the X-ray data of the CeO_2–SrO and CeO_2–CaO systems, respectively. It is seen that the samples of both systems almost attained the theoretical density after sintering at 1450 or 1650° C. These samples had a relative density above 95%. Other samples, i.e. the CeO_2–MgO and CeO_2–BaO systems, also exhibited a high relative density of more than 95%.

3.2. Electrical properties of sintered samples

The ionic conductivities of CeO_2–based oxides measured in air by the d.c. four-probe method are plotted as a function of reciprocal absolute temperature in Fig. 4. The ionic conductivity, σ_i, plotted here is the product of the observed conductivity and the ionic transference number obtained from the e.m.f. of the oxygen concentration cell. Since the ionic transference numbers of CaO- and SrO-doped ceria are almost unity, straight lines are obtained in the log $(\sigma_i T)$ against $1/T$ plots in the temperature range between 500 and 900° C. However, the ionic conductivities of BaO- and MgO-doped CeO_2 were about two orders of magnitude lower than for the CaO- and SrO-doped systems. Their ionic conductivities deviated from straight lines. The ionic conductivity of $(CeO_2)_{1-x}(SrO)_x$ decreased gradually with increasing x, due to the formation of the $SrCeO_3$ phase. On the other hand, the ionic conductivity of CaO-doped CeO_2 was almost constant with an increase in CeO_2

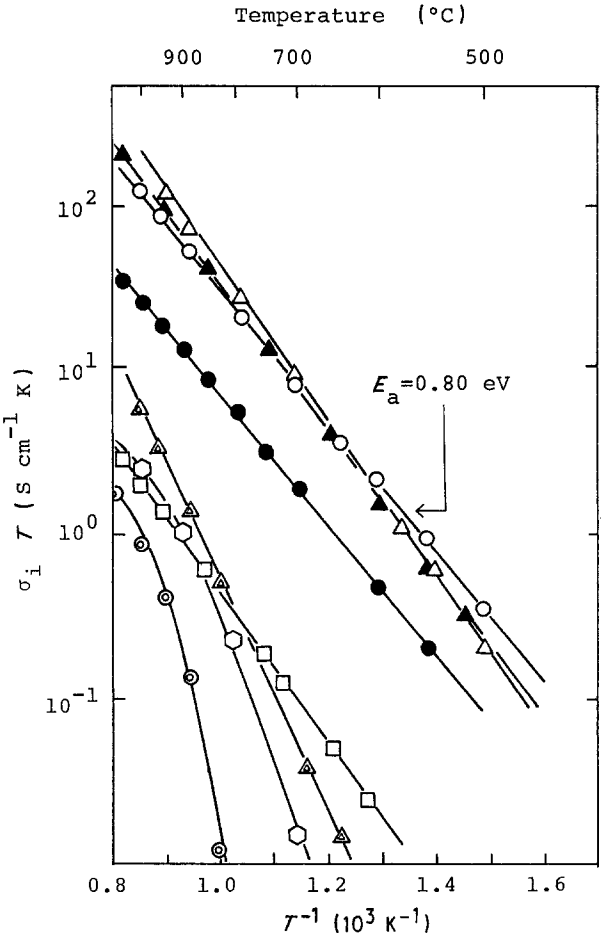

Figure 4 Arrhenius plots of ionic conductivity for (△) $(CeO_2)_{0.90}(CaO)_{0.10}$, (▲) $(CeO_2)_{0.70}(CaO)_{0.30}$, (○) $(CeO_2)_{0.90}(SrO)_{0.10}$, (●) $(CeO_2)_{0.70}(SrO)_{0.30}$, (□) $(CeO_2)_{0.90}(BaO)_{0.10}$, (○) $(CeO_2)_{0.90}(MgO)_{0.10}$, (▲) $(ZrO_2)_{0.85}(CaO)_{0.15}$, (◎) CeO_2.

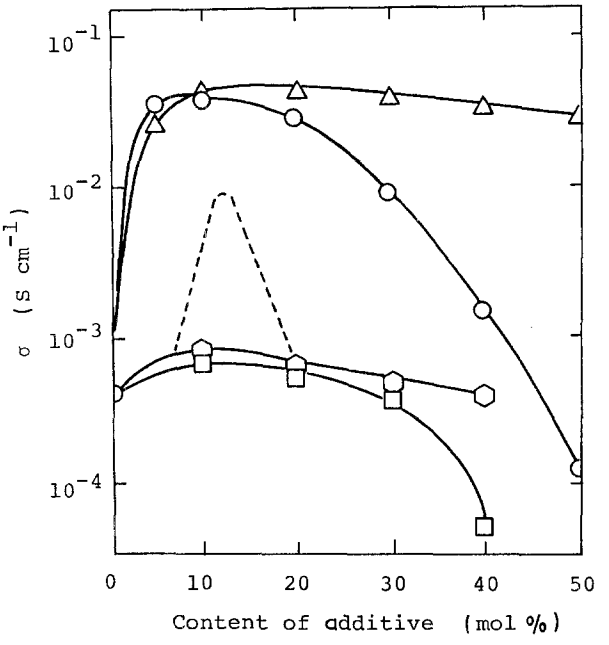

Figure 5 Conductivities of ceria–alkaline earth oxide systems at 800° C as a function of content of dopant: (△) $(CeO_2)_{1-x}(SrO)_x$, (○) $(CeO_2)_{1-x}(CaO)_x$, (□) $(CeO_2)_{1-x}(BaO)_x$, (⬡) $(CeO_2)_{1-x}(MgO)_x$, (– – –) $(ZrO_2)_{1-x}(CaO)_x$ [18].

even though CaO is added after its solubility limit is reached. The ionic conductivities of CaO- and SrO-doped CeO_2 were much higher than those of calcia-stabilized zirconia at every temperature investigated in this study.

The slope of the linear region in the Arrhenius plot gives the apparent activation energy for transfer of the oxygen ion:

$$\sigma_i T = A \exp(-E_a/kT) \quad (3)$$

The activation energies for SrO- and CaO-doped CeO_2 were much smaller than that of calcia-stabilized zirconia. The activation energy for $(CeO_2)_{0.90}(SrO)_{0.10}$ has the value 0.80 eV, which is the lowest in the family of CeO_2–alkaline earth oxide.

Overall electrical conductivities of ceria-based oxides are plotted as a function of the content of added metal oxide in Fig. 5. The conductivities are sharply enhanced by the addition of a small amount of Ca^{2+} and Sr^{2+}, accompanied by the introduction of oxygen vacancies. On the other hand, the conductivities increased only slightly with the addition of BaO and MgO because of their small solubility in CeO_2. The conductivities of $(CeO_2)_{1-x}(CaO)_x$ and $(CeO_2)_{1-x}(SrO)_x$ are obviously higher than that of calcia-stabilized zirconia at the same additive composition. These results confirm the ease of the diffusion of oxygen ions in the cation-doped ceria oxides as compared with stabilized zirconia.

The conductivity of calcia-stabilized zirconia sharply decreased with increasing CaO content at $x > 0.15$. Such a decrease in conductivity is ascribed to defect association and/or concentration-dependent mobilities. On the other hand, the corresponding decreases in conductivity for CeO_2–SrO and CeO_2–CaO after passing through the maximum were only gradual. These decreases in conductivity resulted in the precipitation of second phases. The slope of the decrease for CeO_2–SrO was steeper than that for CeO_2–CaO. This difference is associated with the formation of $SrCeO_3$, whereas in the CeO_2–CaO system no binary compounds are formed.

The ionic transference number of CeO_2–alkaline earth oxide systems was obtained from the e.m.f. of the oxygen concentration cell as a function of temperature. Although the ionic transference number of undoped ceria is only 0.4, those of the CeO_2–CaO and CeO_2–SrO systems were greatly enhanced. The $(CeO_2)_{1-x}(CaO)_x$ and $(CeO_2)_{1-x}(SrO)_x$ samples were regarded as almost pure ionic conductors in a wide composition range ($0 < x < 0.4$) at 600 to 900° C. In the CeO_2–MgO and CeO_2–BaO systems, however, the ionic transference number was less than unity ($t_i = 0.5$ to 0.8), though it was slightly enhanced with the addition of MgO and BaO.

3.3. Microstructure of samples

The microstructures of the CeO_2–SrO system were investigated by X-ray microanalysis. A back-scattered image of $(CeO_2)_{0.70}(SrO)_{0.30}$ is shown in Fig. 6a. Fig. 6b is the Sr$L\alpha$ image of the sample in which bright regions are abundant in strontium. Since the solubility limit of strontia in the ceria lattice is approximately 8 mol %, as mentioned, the sample at $x = 0.30$ contains $SrCeO_3$ as the second phases.

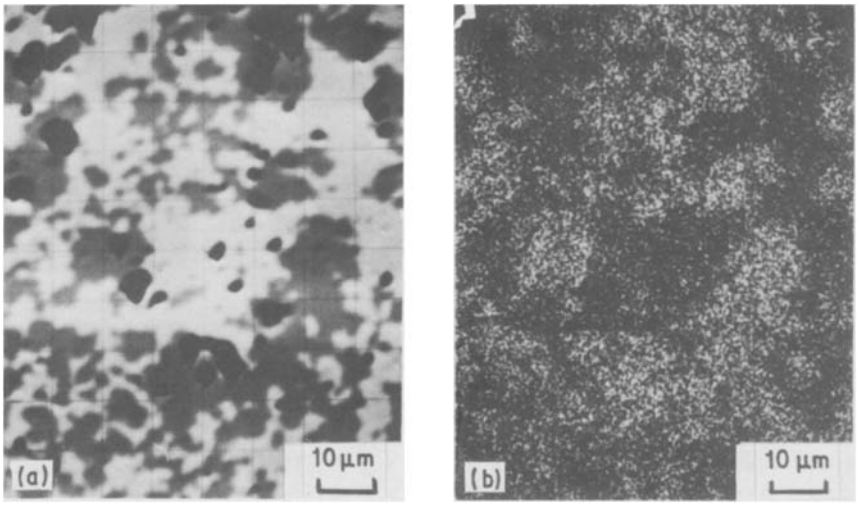

Figure 6 X-ray microanalysis of $(CeO_2)_{0.70}(SrO)_{0.30}$ calcined at 1450° C for 15 h: (a) back-scattered electron image, (b) X-ray image (Sr$L\alpha$).

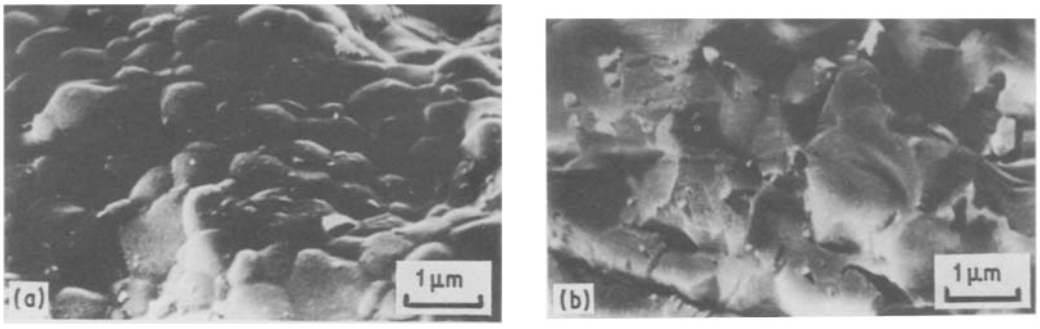

Figure 7 SEM photographs of fractured surfaces of sintered samples from two kinds of oxide precursor: (a) CeO_2–$CaCO_3$ mixture, (b) co-precipitation.

The back-scattered electron image in Fig. 6a consists of bright continuous regions and some dark patches. The back-scattered image of $(CeO_2)_{0.70}(SrO)_{0.30}$ also consists of two kinds of region with different contrast. The X-ray image indicates that the bright region in the back-scattered image is abundant in strontium, and this is attributed to a perovskite phase. The other continuous region is attributed to a solid solution of the fluorite-type oxide. Since the second phase in the CeO_2–SrO and CeO_2–CaO [17] systems is dispersed in the matrix of the fluorite phase, ionic conduction in the solid solution is maintained even above the solubility limit of additives.

3.4. Preparation method of CeO_2–CaO

The effects of the preparation method on the microstructure and electrical properties was investigated by using two oxide precursors; the mixture of commercial CeO_2 and $CaCO_3$ powders, and the co-precipitate from an aqueous solution of $Ce(NO_3)_3$ and $Ca(NO_3)_2$. In the latter case the calculated amount of nitrate salts was dissolved in water, and ammonia water was added to obtain the precipitate. Both precursors were calcined and sintered into discs at 1450° C for electrical measurements. SEM photographs of fractured surfaces of sintered samples from two kinds of oxide precursor are shown in Fig. 7. The microstructure is obviously different between the two methods. The sintered material from the CeO_2–$CaCO_3$ mixture consists of grains with diameter ca. 0.1 to1 μm, and grain boundaries are clearly recognized at the fractured surface. The co-precipitated sample obviously possesses a dense microstructure in which the grain boundaries are not identified clearly. The density of the sintered disc measured from the pycnometric technique was in fact higher for the co-precipitated sample than for the mixture of oxides, in agreement with the SEM observation. This indicates that the preparation by co-precipitation gives well-sintered materials.

Arrhenius plots of the electrical conductivity of samples of the two preparation methods are shown in Fig. 8. The electrical conductivity is largely unaffected by the preparation method; however, the preparation by co-precipitation always gives rise to a slightly higher conductivity than the sample from the CeO_2–$CaCO_3$ mixture. The dense microstructure of co-precipitated samples should be effective in lowering the grain boundary resistance. Since the two oxide components seem to be well mixed and to consist of very fine particles in the co-precipitated precursor, sintering as well as solid-state reaction proceeds easily.

Co-precipitation from nitrate solution was also effective in the preparation of the CeO_2–SrO system. High density and conductivity of sintered discs were similarly attained. Therefore, it is concluded that co-precipitation is a better preparation method for CeO_2–alkaline earth oxides than the mixing of oxides and/or carbonates.

4. Conclusion

Ceria–calcia and ceria–strontia in the ceria–alkaline earth oxide systems of this study showed excellent ionic conductivities and high ionic transference numbers for oxygen. The ionic conductivities of calcia- and strontia-doped ceria were the highest in the family of cation-doped fluorite-type oxides. The cation-doped fluorite phase in the ceria–calcia and ceria–strontia systems is continuous and ionic conduction is scarcely

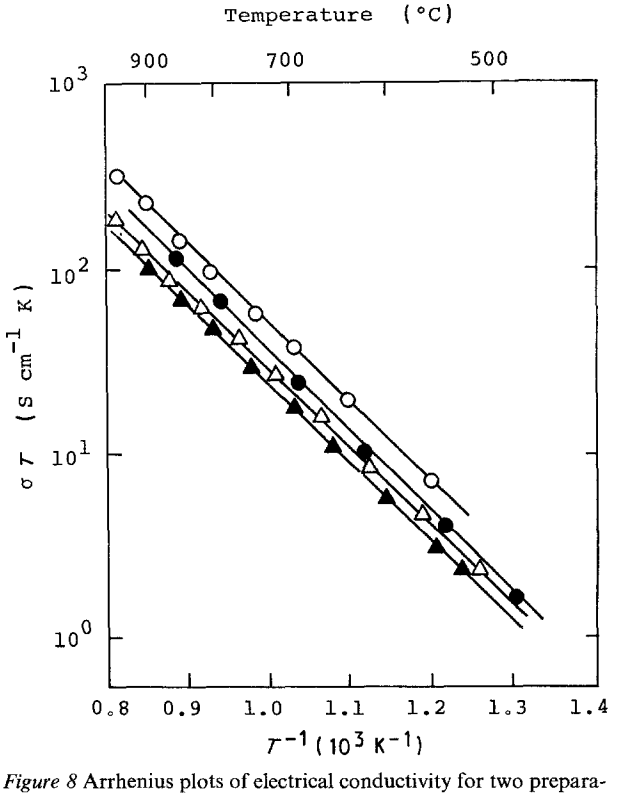

Figure 8 Arrhenius plots of electrical conductivity for two preparation methods: (●) $(CeO_2)_{0.90}(CaO)_{0.10}$ by CeO_2–$CaCO_3$ mixture, (○) $(CeO_2)_{0.90}(CaO)_{0.10}$ by co-precipitation, (▲) $(CeO_2)_{0.90}(SrO)_{0.10}$ by CeO_2–SrO_3 mixture, (△) $(CeO_2)_{0.90}(SrO)_{0.10}$ by co-precipitation.

suppressed, even in the presence of a second phase as observed by X-ray microanalysis. The second phase in both those systems is dispersed in the matrix of fluorite phase, and ionic conduction in the solid solution is maintained even above the solubility limit. For excellent ionic conductivity, calcia- and strontia-doped ceria should be candidates for the oxide electrolyte material of the third-generation fuel cell.

Acknowledgement

The authors wish to express their thanks to Professor F. Hirowatari and Dr N. Shimada for their experimental support in the X-ray microanalysis measurements.

References

1. T. TAKAHASHI, K. ITO and H. IWAHARA, *Denki Kagaku* **34** (1966) 205.
2. T. L. MARKIN, R. J. BONES and R. M. DELL, in "Superionic Conductors", edited by G. D. Mahan and W. L. Roth (Plenum, New York, 1976) p. 15.
3. R. T. DIRSTINE, W. D. GERTRY, R. N. BLUMENTHAL and W. HAMMETTER, *Ceram. Bull.* **58** (1979) 778.
4. A. S. NOWICK and D. S. PARK, in "Superionic Conductors", edited by G. D. Mahan and W. L. Roth (Plenum, New York, 1976) p. 395.
5. C. B. CHOUDHARY, H. S. MAITI and E. C. SUBBARAO, in "Solid Electrolytes and Their Applications", edited by E. C. Subbarao (Plenum, New York, 1980) p. 1.
6. S. H. CHU and M. A. SEITZ, *J. Solid State Chem.* **23** (1978) 297.
7. E. C. SUBBARAO and H. S. MAITI, *Solid State Ionics* **5** (1981) 539.
8. H. ARAI, T. KUNISAKI, Y. SHIMIZU and T. SEIYAMA, *ibid.* **20** (1986) 241.
9. J. E. GARNIER, R. N. BLUMENTHAL, R. J. PANLENER and R. K. SHARMA, *J. Phys. Chem. Solids* **37** (1976) 369.
10. H. YAHIRO, K. EGUCHI and H. ARAI, *Solid State Ionics* **21** (1986) 37.
11. R. N. BLUMENTHAL and J. E. GARNIER, *J. Solid State Chem.* **16** (1976) 21.
12. D. Y. WANG and A. S. NOWICK, *ibid.* **35** (1980) 325.
13. T. KUDO and H. OBAYASHI, *J. Electrochem. Soc.* **122** (1975) 142.
14. R. T. DIRSTINE, R. N. BLUMENTHAL and T. F. KUECH, *ibid.* **126** (1979) 264.
15. R. GERHARDT and A. S. NOWICK, *J. Amer. Ceram. Soc.* **69** (1986) 641.
16. V. LONGO and L. PODDA, *ibid.* **61** (1978) 371.
17. K. EGUCHI, T. KUNISAKI and H. ARAI, *Commun. Amer. Ceram. Soc.* **69** (1986) 282.
18. T. TAKAHASHI, in "Physics of Electrolyte", edited by J. H. Ladik (Academic, New York, 1972) p. 989.

Received 26 May
and accepted 24 July 1987